The 2nd to 4th century explosive activity of Vesuvius: new data on the timing of the upward migration of the post-A.D. 79 magma chamber

Raffaello Cioni[1,*], Claudia D'Oriano[2], Antonella Bertagnini[2], Daniele Andronico[3]

[1] Università di Cagliari, Dipartimento di Scienze della Terra, Cagliari, Italy

[2] Istituto Nazionale di Geofisica e Vulcanologia, Sezione di Pisa, Pisa, Italy

[3] Istituto Nazionale di Geofisica e Vulcanologia, Sezione di Catania, Osservatorio Etneo, Catania, Italy

ABSTRACT

We present volcanological data on the deposits of the Santa Maria Member (SMM), the eruption cycle occurred at Vesuvius (Italy) in the period between the A.D. 79 plinian and the A.D. 472 subplinan eruptions. Historical accounts report only sporadic, poorly reliable descriptions of the volcanic activity in this period, during which a stratified sequence of ash and lapilli beds, up to 150 cm thick, with a total volume estimated around 0.15 km³, was widely dispersed on the outer slopes of the volcano. Stratigraphic studies and component analyses suggest that activity was characterized by mixed hydromagmatic and magmatic processes. The eruption style has been interpreted as repeated alternations of continuous and prolonged ash emission activity intercalated with short-lived, violent strombolian phases. Analyses of the bulk rock composition reveal that during the entire eruption cycle, magma maintained an homogeneous phonotephritic composition. In addition, the general trends of major and trace elements depicted by the products of the A.D. 79 and A.D. 472 eruptions converge to the SMM composition, suggesting a common mafic endmember for these eruptions. The volatile content measured in pyroxene-hosted melt inclusions indicates two main values of crystallization pressures, around 220 and 70 MPa, roughly corresponding to the previously estimated depth of the magma reservoirs of the A.D. 79 and A.D. 472 eruptions, respectively. The study of SMM eruption cycle may thus contribute to understand the processes governing the volcano reawakening immediately after a plinian event, and the timing and modalities which govern the migration of the magma reservoir.

Introduction

The last 4000 years of activity of Somma-Vesuvius have been characterized by frequent eruptive events of largely variable scale, from plinian to violent strombolian, up to quiet lava effusions. Starting from the Avellino plinian eruption (3.9 ka BP) [Sulpizio et al. 2010a], the activity became more and more frequent, while, on average, the intensity of each event occurring in the periods between the largest eruptions, progressively decreased [Cioni et al. 2008, Santacroce et al. 2008]. After the A.D. 79 Pompeii eruption, two main subplinian eruptions occurred (A.D. 472 Pollena and A.D. 1631), spaced out by periods of prolonged, less intense activity. As a general rule, major eruptions were preceded by quiescent periods from several decades to several centuries and, conversely to what had usually happened for the oldest eruptions, they were rapidly followed by a renewal of the activity. The record of all these events is well preserved in the stratigraphy of the volcano, especially for the products of the pyroclastic eruptions.

Volcanological studies at Vesuvius have been mostly concentrated on the products of the largest eruptions [Lirer et al. 1973, Rosi and Santacroce 1983, Sigurdsson et al. 1985, Rolandi et al. 1993, Cioni et al. 1995, Cioni 2000, Sulpizio et al. 2005, Sulpizio et al. 2010a,b, Mele et al. 2011], while, more recently, a renewed interest arose also on the minor eruptions [Rolandi et al. 1998, Marianelli et al. 1999, Arrighi et al. 2001, Andronico and Cioni 2002, Cioni et al. 2011, D'Oriano et al. 2011]. In particular, the study of the activity that characterized the period separating two major eruptions, assumes a certain importance as it can help in explaining the way of transition from low to high intensity eruptions, and *vice-versa*.

After the A.D. 79 eruption, only sporadic direct information from historical sources is available on eruptive activity and the state of the volcano. In this paper we focus on the products of an eruption cycle, interbedded between the two major eruptions of A.D. 79 and 472, and indicated in the volcanological map of
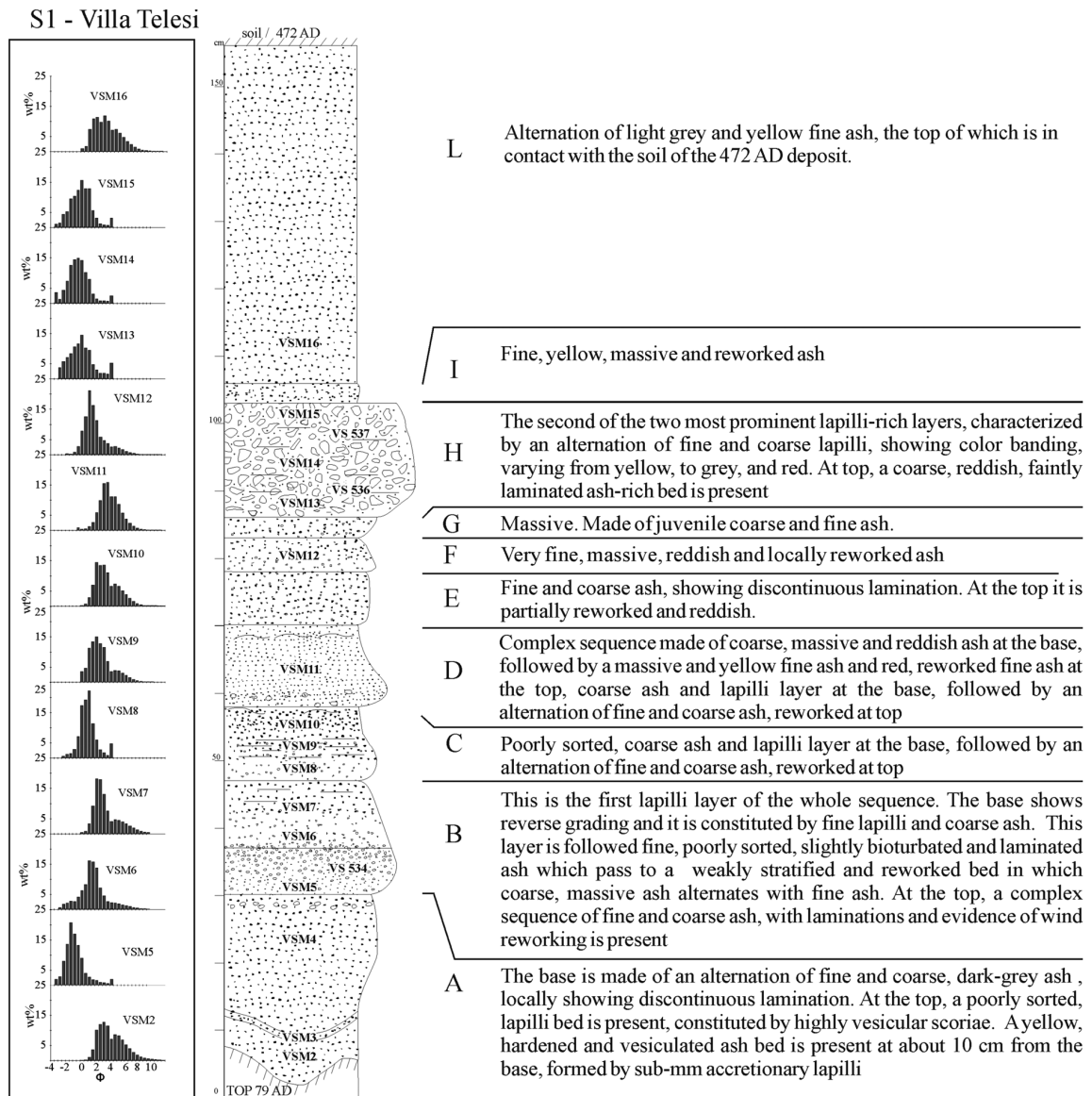
S1 - Villa Telesi

L Alternation of light grey and yellow fine ash, the top of which is in contact with the soil of the 472 AD deposit.

I Fine, yellow, massive and reworked ash

H The second of the two most prominent lapilli-rich layers, characterized by an alternation of fine and coarse lapilli, showing color banding, varying from yellow, to grey, and red. At top, a coarse, reddish, faintly laminated ash-rich bed is present

G Massive. Made of juvenile coarse and fine ash.

F Very fine, massive, reddish and locally reworked ash

E Fine and coarse ash, showing discontinuous lamination. At the top it is partially reworked and reddish.

D Complex sequence made of coarse, massive and reddish ash at the base, followed by a massive and yellow fine ash and red, reworked fine ash at the top, coarse ash and lapilli layer at the base, followed by an alternation of fine and coarse ash, reworked at top

C Poorly sorted, coarse ash and lapilli layer at the base, followed by an alternation of fine and coarse ash, reworked at top

B This is the first lapilli layer of the whole sequence. The base shows reverse grading and it is constituted by fine lapilli and coarse ash. This layer is followed fine, poorly sorted, slightly bioturbated and laminated ash which pass to a weakly stratified and reworked bed in which coarse, massive ash alternates with fine ash. At the top, a complex sequence of fine and coarse ash, with laminations and evidence of wind reworking is present

A The base is made of an alternation of fine and coarse, dark-grey ash, locally showing discontinuous lamination. At the top, a poorly sorted, lapilli bed is present, constituted by highly vesicular scoriae. A yellow, hardened and vesiculated ash bed is present at about 10 cm from the base, formed by sub-mm accretionary lapilli

Figure 1. Stratigraphic section of SMM deposit at S1- Villa Telesi outcrop. The different units are indicated, from the base to the top, with the labels A-L. Pictures correspond to the main units and show the position of collected samples. Grain size analyses for the different samples were performed by mechanical agitation at whole Φ intervals, from −4 to 3 Φ, and for intervals from 3 to 12 Φ using a laser particle size analyzer at the Geography Department of Coventry University (UK).

Figure 2. The depositional features of SMM eruption cycle at S1 (Villa Telesi stratigraphic section). Fa, fine-grained ash; Ca, coarse-grained ash; Fl, fine-grained lapilli; Cl, coarse-grained lapilli.

Mt. Somma-Vesuvius [Santacroce et al. 2003] as the Santa Maria Member (SMM), named, basing on a "type locality" criterion, from the village of Santa Maria la Scala (in the municipality of San Giuseppe Vesuviano), where these products are best exposed.

The SMM consists of a finely stratified ash fallout sequence interlayered with some lapilli beds (Figures 1, 2), which is mainly distributed on the volcano's flanks, and sporadically present also in the surrounding plain (Figure 3). Even if lava flows are not preserved in the volcanic successions, effusive activity might have been important during this period, being possibly confined inside the pre-existing, post-A.D. 79, summit caldera depression [Cioni et al. 1999b]. The products of this activity have been briefly described in some preceding papers; Arnò et al. [1987] mentioned these deposits, without
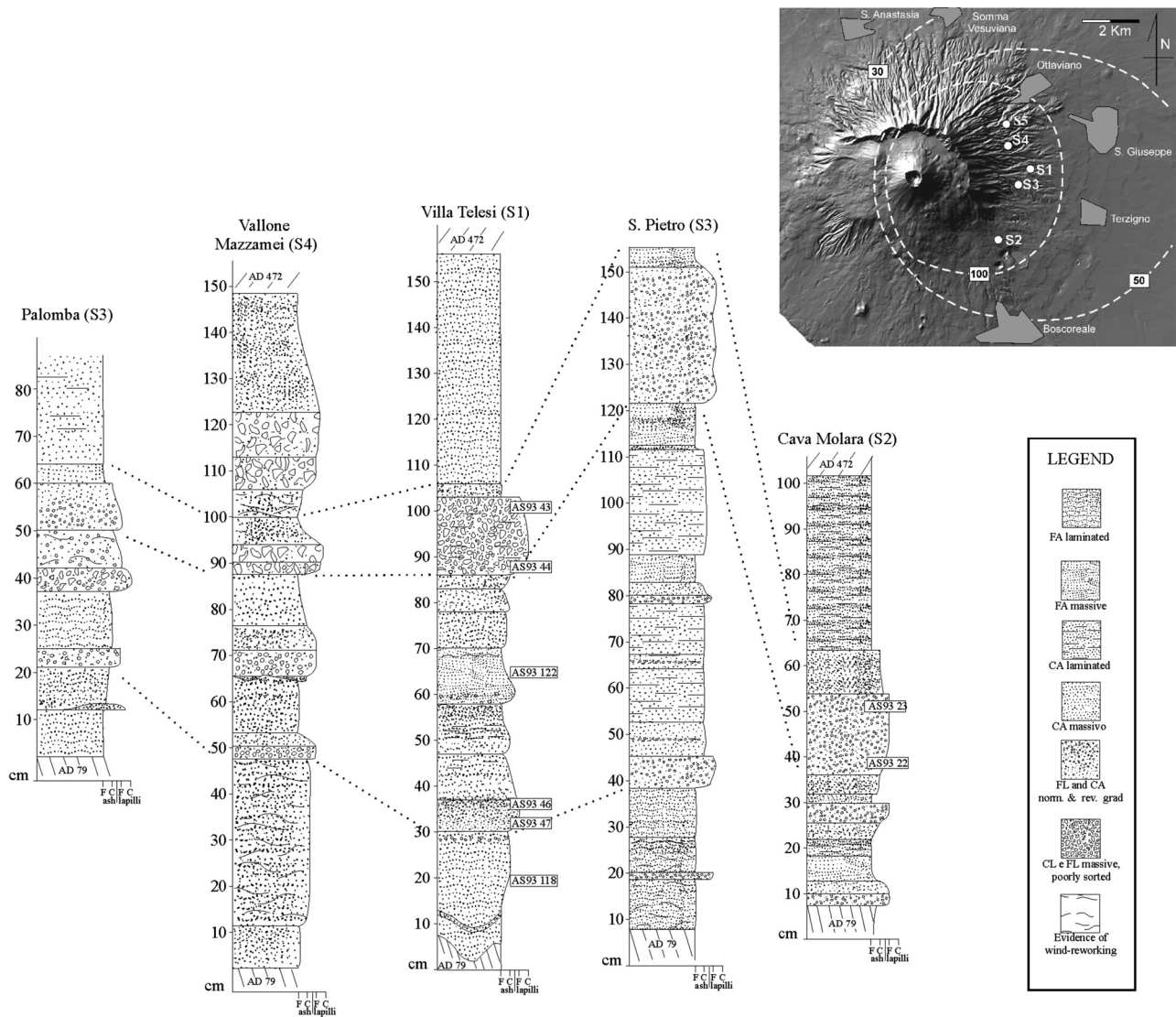
Figure 3. Lateral stratigraphic variations between the main sections of SMM deposits. The inset in the right upper corner shows the dispersal of the total deposit and the locations of the studied sections.

providing a detailed stratigraphic and petrochemical descriptions. They only described a thin scoria lapilli bed cropping out near Somma Vesuviana, and a dubious lahar/pyroclastic flow deposit underlying the deposits of the Pollena eruption at Terzigno and along the inner portion of the caldera wall. In a paper focused on the interplinian activity of the last 3500 years of Somma-Vesuvius, Rolandi et al. [1998] concisely described the products of the A.D. 79-472 period, mainly giving a detailed historical account from different sources.

In the following, we present a detailed description of the deposits of SMM eruption cycle, aimed at interpreting the style of activity, the geochemical characteristics of the products and the compositional relationships of the SMM products with those of the A.D. 79 and A.D. 472 major eruptions.

The study of the SMM products assumes a remarkable importance for the comprehension of the volcanic hazard in the Vesuvian area, as it may contribute to the understanding of the processes governing the vol-

cano and its shallow magmatic system immediately after a paroxysmal event, and in correspondence of a major change in the depth of the magma chamber system [Scaillet et al. 2008].

Historical accounts

Historical accounts on Somma-Vesuvius post-A.D. 79 activity were summarized by Principe et al. [2004], in the review of Alfano [1923] and in Rolandi et al. [1998]. After the A.D. 79 Pompeii eruption, the first mention to a renewed Vesuvius activity was by Galenus [1609] in the work *De methodo medendi*. His phrase, related to the Vesuvius state during A.D. 172 – "quae nunc etiam uritur" ["that still now it is burned"] – suggests that at that time the volcano was possibly active. In his *Historia Romana*, Dio Cassius reported that in A.D. 203 he saw from Capua "a very large fire that burned", followed by "strong rumbles". In the same work, he also reported notice of frequent (every year) activity in the period between A.D. 222 and A.D. 235. Controversial, equiv-

ocal information about the state of the volcano comes from Pacianus [Alfano and Friedlaender 1929], who reported that between the A.D. 379 and the A.D. 395, Mt. Vesuvius, together with Mt. Etna and Stromboli, was considered a proof of the existence of the fire of the Hell, showing an activity characterized by fumaroles and real eruptions.

Rolandi et al. [1998] also mentioned two other sentences from later authors, to which however scarce credibility is given; one from Maiolo [1615], stating that "a lava flow was stopped by Saint Januarius in the A.D. 305 under the empire of Diocletianus", and another reported in the *Theatrum Vitae Humanae*, also cited by following authors as Mecatti [1754] and Palmieri [1887], according to which in the A.D. 321 "Vesuvius burnt and ejected for some days lava and ash".

Even though it is not clear what was the shape of the volcano before the paroxysmal A.D. 472 eruption, Dio Cassius, speaking about the shape of the volcano in the years between the A.D. 222-235, describes an amphitheater-like summit ("totus mons… formam habent amphitheatri"). These few data from coeval accounts suggest that the volcanic activity of Mt. Vesuvius between A.D. 79 and A.D. 472 was nevertheless relevant and maybe quite continuous at least over some decades, with a possible occurrence of a paroxysm in the A.D. 203, followed by volcanic activity until at least A.D. 235, and a quiescence period preceding the A.D. 472 Pollena eruption, probably not longer than a couple of centuries.

Stratigraphy

The best and most complete exposition of the SMM deposits is located in proximity of the Santa Maria la Scala village, where they reach the maximum thickness of about 150 cm. We propose the Villa Telesi section (Figures 1, 2), at 220 m a.s.l. and 4 km eastward from the vent, as the type locality for the SMM deposits. Here, they appear as a complex sequence of laminated ash and minor lapilli beds. The laminated ash beds generally consist of millimetric alternations of fine and coarse ash, often convoluted by loading. The presence of shortly spaced wavy, poorly continuous laminations, or cross beddings suggest the occurrence of local reworking by wind or localized sheet-wash. All the recognized lapilli beds are quite similar, and mainly formed by yellow-brown, vesicular, sub-centimetric scoriae, with microphenocrysts of leucite and pyroxene and only minor phlogopite. Lithic fragments are rare and generally represented by lava fragments. Loose crystals of leucite and pyroxene are always present, although scarce. The depositional mechanism responsible of the emplacement of the entire sequence was the fallout from lava fountains (lapilli beds) with associated plumes rising up to some kilometers, and from ash plumes dispersed by low-level winds (ash-rich beds).

The SMM sequence is separated by an erosive unconformity from the deposit of the final phase of the A.D. 79 Pompeii eruption (Figure 3). This latter consists of light colored, accretionary lapilli-bearing, phreatomagmatic ash, often accumulated into metric sized, V-shaped gullies cut in the underlying cohesive ash, and probably due to extensive, generalized flooding. The contact between the A.D. 79 and the SMM deposits is often marked by a thin, light colored, indurated ash layer, marking a weathering surface. No evidence of paleosol or humic materials has been ever found at the base of the SMM. On the contrary, at the top, the SMM deposits have a well-developed, light brown, darkening upward paleosol, with thickness up to 30 cm. This is followed, in the eastern and north-eastern sectors of the volcano, by the characteristic fallout scoria blanket of the A.D. 472 Pollena eruption [Rosi and Santacroce 1983, Sulpizio et al. 2005].

The SMM sequence was subdivided into 10 units (according to the nomenclature proposed by Jenkins et al. [2007]), each including a single eruption event, which probably lasted from several days to few months. The identification of the different units is based on the recognition of minor discontinuities resulting from prolonged pauses in the deposition, such as pedogenized or weathered surfaces and secondary erosions, represented by small scale erosive scours on the ash. Eruption events consist of successions of different stages that led to the deposition of basal lapilli beds, followed by one or more laminated ash beds, and topped by a massive, locally reworked ash bed (Figures 1, 2, 3).

Fifteen samples, labeled VSM2 - VSM16 from the base to the top, were collected along the whole succession, and used for grain size, textural and compositional analyses. Grain size analyses of samples collected at Villa Telesi (S1) show unimodal trends and well sorted distributions for the lapilli beds, with the mode that varies from -1 Φ at the base (Unit B) to 1 Φ (Unit C) to 0 Φ at the top (Unit H). Ash-rich layers are generally characterized by bimodal size distribution, with the first principal peak that varies between 1-3 Φ and a second peak constant at 4.5 Φ.

Dispersal and volume

The SMM deposits are mainly distributed in the eastern sector of the volcano. The thickness of the entire succession shows a rapid downwind thinning, from about 150 cm at 4 km from the vent, to no more than 50 cm at a distance of 8-10 km (Figure 3). Minor, scattered outcrops have been surveyed both along the north-western flank, near the Lagno di Pollena, and in

several sites of the south-eastern sector of the volcano. The two main lapilli beds (Units B and H) are easily correlated throughout the dispersal area, allowing the reconstruction of the dispersal directions of these main beds. Conversely, the ash-rich layers are affected by thickness variation and inner structures that make difficult a layer-to-layer correlation (Figure 3). In general, the SMM deposits show an overall large, nearly circular, eastward shifted dispersal, that can be related to the prolonged duration of the activity, during which ash dispersal was affected by variable wind conditions. The large crosswind range of the isopachs with respect to the downwind range is a further confirmation that the isopach map of the total deposit of Figure 3 is the result of the superposition of multiple fallout beds, each showing a slightly different direction of the dispersal axis.

A rough estimation of the total volume of the erupted products was obtained using the method of Pyle [1989], with the formulation of Fierstein and Nathenson [1992], resulting in a total volume around 0.15 km^3.

Analytical methods

Clast morphology
The morphological features of the juvenile fragments were investigated at the electron microscope laboratories of the University of Pisa, Dipartimento di Scienze della Terra, and of the Istituto Nazionale di Geofisica e Vulcanologia (INGV), Pisa and Rome sections. Up to 50-100 clasts, from both the main lapilli beds (Units B and H) and from two ash-rich layers (Units A and D), were selected for SEM inspection. For each sample, two different size intervals (1Φ and 3Φ) were considered. The choice of these grain sizes was based on the mode of the selected samples (1Φ for VSM6 and VSM15; and 3Φ for the VSM5 and VSM11). Juvenile fragments were hand picked, fixed on aluminium stubs with conductive glue, and carbon coated. Before gluing, fragments were rinsed in distilled water and washed in an ultrasonic bath for a maximum of 30 s, in order to avoid the formation of secondary cracks on the particles [Cioni et al. 1992]. SEM observations included description of particle shape, vesicularity (according to Houghton and Wilson [1989]), external surface texture, and possible occurrence of surface alteration or secondary minerals [Wohletz 1983, Heiken and Wohletz 1991, Cioni et al. 1992].

Composition
Centimeter-sized juvenile scoriae from the two main lapilli layers were sampled for bulk rock analyses (Table 1). Samples were powdered in agate jars and analyzed for major via XRF spectrometry, with a Philips

PW1480 spectrometer at the Dipartimento di Scienze della Terra (University of Pisa). Trace elements were determined by Neutron activation analyses (INAA) according to the method of Joron et al. [1997] at CEA/CNRS Saclay (France; analyst J.L. Joron).

Major elements in residual glasses of ash fragments were measured at INGV-Rome with a Jeol-JXA8200 EMP, equipped with five wavelength-dispersive spectrometers, using 15 kV accelerating voltage and 10 nA beam current. Analyses were performed with a defocused electron beam of 5 μm and a counting time of 5 s on background and 15 s on peak.

Fifteen large (more than 30 μm) and glassy melt inclusions (MI) trapped in clinopyroxene phenocrysts were selected from three samples representative of the basal (VS 543, Unit B) and topmost parts (VS536 and VS537, respectively the base and top of Unit H) of the stratigraphic succession and studied for major and trace elements composition and for the measurement of H_2O and CO_2 contents. Major elements in MI and hosting mineral were determined with a WDS JEOL JXA 8600 electron microprobe at IGG-CNR of Florence, at 15 kV accelerating voltage and 10 nA defocused beam. Trace elements were analyzed at the Dipartimento di Scienze della Terra of Cagliari by using a Laser ablation ICP-MS device, operating at 10 Hz of repetition rate, a laser output energy of 0.28 mJ, spot size of 30-35 μm and He as carrier gas in the ablation cell [D'Oriano et al. 2008]. Selected elements were acquired in peak hopping mode with a dwell time of 10 ms. Nist 612 and ^{44}Ca were adopted as external and internal standards, respectively. Data reduction was performed by means of GLITTER® software (Macquarie Research Ltd.; http://www.glitter-gemoc.com/) developed by van Achterberg et al. [2001].

On each MI either 2 or 3 analyses were performed by FTIR microspectroscopy, with a Nicolet Magna 560 spectrometer equipped with a NicPlan infrared microscopy (Dipartimento di Scienze della Terra, University of Pisa). The methods of melt inclusion preparation for FTIR analysis and recalculation are described in Cioni [2000], using a glass density of 2700 g/cm^3.

Morphology of the juvenile clasts
The analysis of the morphological features of juvenile clasts is a valid tool for reconstructing the modalities of magma vesiculation and fragmentation during explosive eruptions [Heiken and Wohletz 1985]. In particular, morphological analyses have been often performed to infer the style of fragmentation and especially the active involvement of external fluids (phreatic or surface water, steam) in the eruption dynamics [Wohletz 1983, Cioni et al. 1992, Dellino and La Volpe 1996].

Morphological analyses of juvenile clasts were per-

Sample	Unit B			Unit H			
	VSM5	AS93 47	AS93 46	AS93 44	AS93 43	AS 93 22	AS 93 23
SiO_2 (wt%)	49.12	50.81	50.13	49.93	49.6	49.26	48.91
TiO_2	0.75	0.81	0.83	0.86	0.84	0.89	0.88
Al_2O_3	15.66	16.13	16.19	15.83	16.11	16.49	16.51
Fe_2O_3	6.69	7.3	7.65	7.87	7.73	8.22	8.26
MnO	0.14	0.14	0.15	0.15	0.15	0.16	0.16
MgO	4.84	5.07	5.07	5.13	4.99	5.37	4.89
CaO	9.37	9.11	9.05	9.81	9.66	9.38	9.2
Na_2O	2.84	2.81	2.95	2.73	2.77	2.67	2.77
K_2O	7.12	7.22	7.4	7.06	7.53	6.89	7.79
P_2O_5	0.62	0.61	0.59	0.65	0.63	0.69	0.65
Sc (ppm)	20.0	18.7	18.8	20.7	18.9	21.0	20.0
Cr	140	139	148	132	114	142	135
Co	25.0	24.2	24.2	25.7	24.2	25.0	25.8
Ni	50.0	49.0	46.0	45.0	40.5	44.4	44.0
Rb	285	266	264	259	254	239	268
Sr	956	927	972	1023	1013	966	1056
Zr	210	235	216	217	209	207	233
Sb	bdl	0.58	0.57	0.57	0.51	0.49	0.61
Cs	15.20	15.39	15.11	14.01	13.80	13.08	14.43
Ba	1734	1664	1713	1821	1790	1706	1903
La	59.20	56.65	57.30	53.63	57.30	54.30	55.21
Ce	111.0	113.6	114.7	110.8	108.9	106.0	116.1
Sm	8.22	8.45	8.60	8.92	8.64	9.02	9.03
Eu	2.21	2.45	2.25	2.50	2.35	2.36	2.45
Tb	0.91	0.79	0.81	0.84	0.82	0.83	0.84
Yb	1.98	2.00	2.09	2.06	2.05	2.03	2.07
Hf	4.30	4.52	4.48	4.60	4.46	4.37	4.70
Ta	1.99	1.93	2.00	2.02	1.99	1.88	2.10
Th	21.90	22.24	22.85	21.41	21.22	19.84	22.47
U	8.49	7.95	8.16	8.09	8.13	7.49	8.61

Table 1. Bulk rock compositions of coarse scoriae collected at S1 and S3 from the main lapilli layers. Sample's position is indicated in Figures 1-3.

formed both on the lapilli and ash beds; in the following, we present separately the results obtained for the two types of deposits.

The lapilli beds

Clasts from the two main lapilli beds (Units B and H) were analyzed. Fragments in the 1Φ size interval have a general fresh aspect, and, on average, clasts related to the two beds are quite similar. The main differences consist in a slight increase of clast vesicularity passing from Unit B to Unit H, and in the occurrence of a poorly developed ash coating on the fragments of

Unit B. In general, external surfaces of the clasts are glassy, with predominant smooth and fluidal aspect. Clast morphology varies between sub-equant sub-angular to tubular, with sharp edges (Figure 4a,b,c) and fluidal external surfaces (Figure 4e,f,g). Thin, small glass threads or filaments sometimes protrude from these surfaces, especially in the tubular clasts (Figure 3g). The globular protrusions visible on some fragments (Figure 4f) are related to leucite microphenocrysts. Blocky clasts are rare. Clast vesicularity varies from high to intermediate (Figure 4a) with a bubble size range rather limited, being the mean diameter between

50 and 100 microns (Figure 4a,b,c,d). Vesicles are spherical or slightly oblate (Figure 4b,c,d), and separated by septa not larger than a few tens of microns.

Fragments from the finer grain size (3Φ) show a similar glassy appearance. They are characterized by irregular spongy and fluidal surfaces, and rare blocky shapes (Figure 4h). Blocky fragments are more abundant in Unit B, while in unit H spongy clasts are predominant. Vesicularity is characterized by sub-rounded bubbles of uniform size, separated by thin walls, with a low degree of bubble coalescence.

The ash beds

Juvenile fragments from two ash beds (Units A and D) were analyzed. Differently from the lapilli beds, fragments from ash beds show a larger variability of the morphological features. Ash clasts from the lower bed (Unit A) are mostly equant and blocky (Figure 5). Clasts with irregular, spongy and fluidal shapes, although in limited amount, are also present (Figure 5d). Fragments are characterized by not-pristine external surfaces (Figure 5a), showing a continuous layer, a few microns thick, characterized by secondary minerals that simulate a diktytaxitic texture [Heiken and Wohletz 1985] (Figure 5b), which consists of a network of crystals (clinopyroxene and leucite) enclosing angular voids (Figure 5c). Clasts showing glass alteration generally present also an intense ash coating on the external surfaces and an important ash infilling of the vesicles (Figure 5d,e). Aggregates of fine ash (<10 microns) are common in the basal ash bed.

Juvenile clasts from Unit D, instead, have mostly fresh, glassy and smooth surfaces, with some minor fragments showing rough, altered surfaces. The shape of the ash fragments varies from blocky to oblate, with smooth, fluidal surfaces (Figure 5d,h). Non fluidal fragments are generally angular to subangular (Figure 5g).

For both samples, clast vesicularity varies from low to intermediate (Figure 5g,h). The pumice-like, spongy fragments which characterize the lapilli beds, are here totally lacking. Vesicles show a large size variability, having the mean diameter between few tens and hundred microns, and are characterized by ellipsoidal and generally deformed shapes (Figure 5h). In agreement with the low vesicularity of the clasts, thick septa separate the vesicles. This reflects in the large abundance of blocky fragments in the finer material. Loose crystals covered by a glass veneer occur in the finer size range, in particular in Unit D.

Petrography

Juvenile material from the lapilli beds (Units B and H) consists of low porphyritic, glassy scoriae with rare phenocrysts of colorless to light green clinopyroxene
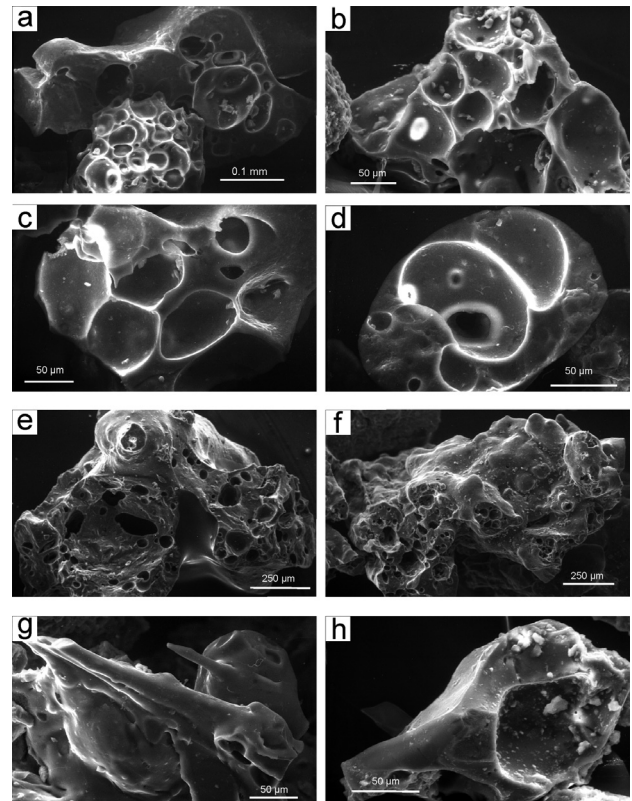

Figure 4. SEM images of ash fragments in the lapilli beds (AS 95 44 and 47), showing the morphological features.
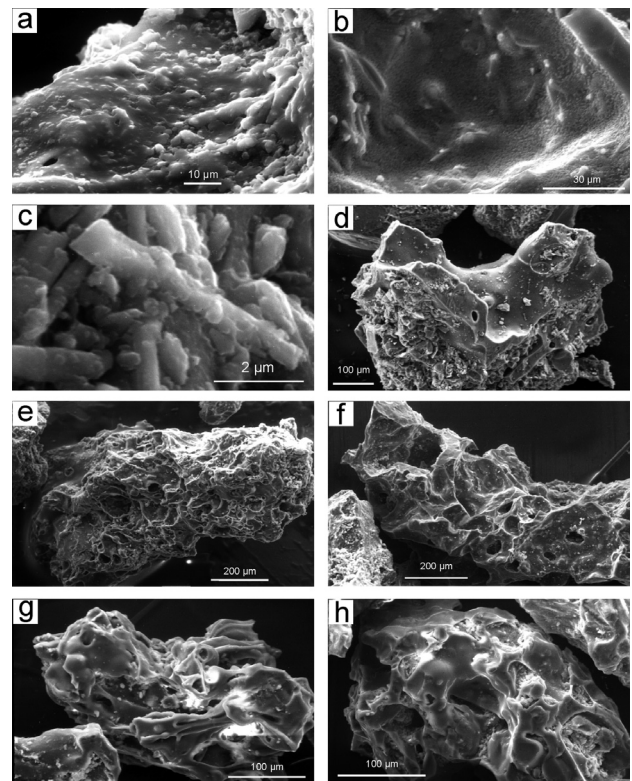

Figure 5. SEM images of the ash fragments in the ash layers (AS 95 118 and 122), showing the main feature of the clasts morphology.

(cpx) and leucite (lct). Scoriae from the upper lapilli bed (Unit H) contain also phlogophite as phenocryst. Cpx phenocrysts are characterized by oscillatory zoned rims
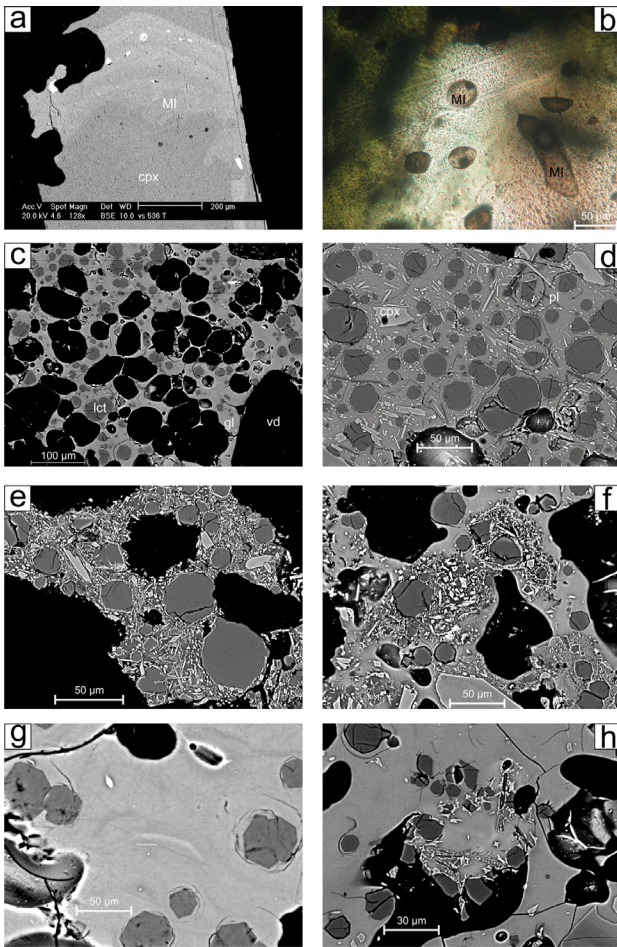
Figure 6. A random selection of about 30 fragments for sample, in the size 1 Φ and 3 Φ size intervals, was considered for the petrographical characterization (vesicularity, crystal-content, texture). Backscattered (BSE) images were captured with scanning electron microscopy (SEM) at Istituto Nazionale di Geofisica e Vulcanologia (Pisa) using a Zeiss EVO-MA-10 working at accelerating voltage 15 kV and distance 10 mm. a) BSE image of a pyroxene phenocryst characterized by a large, resorbed core and complex oscillatory rim. Trapped melt inclusions are visible at the border between the core and rim; b) optical microscope image of pyroxene phenocryst with many brown, round melt inclusions. c-d-e-f-g-h represent BSE images, showing the main textural features of: c) a vesicular, glassy ash fragment from the VSM5 sample; d) a low vesicular, intermediate crystal-rich ash fragment from VSM 5 sample; e) dense, crystal rich fragment from VSM11 sample; f) dense, crystal rich portion of clasts included in a glassy groundmass; g) chaotic texture of two glasses with different composition in VSM 5 sample; h) two glasses with different compositions separated by quenching microlites. cpx, clinopyroxene; MI, melt inclusion; V, vesicles; gl, glass; lct, leucite; pl, plagioclase.

and may present skeletal to complexly resorbed cores, which often occupy more than 50 vol% of the crystals (Figure 6a,b). They show a diopsidic to salitic composition (Fs_{5-16} En_{34-49} $Wo_{50.5-52}$), and are very similar to type 5 cpx described by Cioni et al. [1998], which characterize samples from some other mid-intensity Vesuvius eruptions (AP4, A.D. 472, A.D. 1906). The large crystals in many cases host melt inclusions with faceted or ellipsoidal shape, which often form a trail along the border between zones of the crystal with different com-

position. Melt inclusions are generally less of 50 microns across, and are characterized by small shrinkage bubbles (Figure 6a,b).

The groundmass has a largely variable microlite content, from about 30-40 vol% up to nearly holocrystalline (Figure 6c,d,e). Lct is the main phase present in the groundmass of highly vesicular fragments, where it is associated with minor pyroxene, plagioclase (pl), apatite and rare Fe-Ti-oxide in the most crystal-rich products (Figure 6e). Microlites of lct are idiomorphic, sometimes showing a clustered texture, and are generally bordered by concentric contraction fractures (Figure 6d). Cpx microlites are characterized by euhedral, tabular habit and are compositionally zoned, with the same compositional range shown by phenocrysts (Figure 6d). The smaller crystals can exhibit swallowtail morphologies or hopper texture, in response to rapid growth during the late stage of crystallization. Sometimes, pyroxene microlites in scoriae from the lapilli layers are arranged with a fluidal pattern (Figure 6d). Euhedral microlites of pl occur in the groundmass; they have homogeneous size (10-30 micron), and faceted, tabular habitus (Figure 6d), suggesting a high growth rate and intermediate undercooling [Hammer and Rutherford 2002]. They are scarce in the ash layer at the top of the sequence. In backscattered electron microscope images, micro-scale mingling textures are often observed in the groundmass glass of the fragments from the ash beds. In particular, zones with chaotically arranged, dark glass filaments are observed in a gray glassy groundmass (Figure 6g) together with portions of glass bordered by quenching crystals of pl (Figure 6h).

Dense, felty textured, holocrystalline scoriae are present especially in the ash beds both as single fragments and as small inclusions in the highly vesicular, glassy fragments (Figure 6f). In these fragments, round vesicles smaller than 5 μm are scattered in the residual glass, possibly reflecting the latest stages of vesiculation following massive groundmass crystallization.

Chemistry

Whole rock

Scoriae collected from the different beds show homogeneous bulk rock composition, falling in the phonotephrite compositional field (SiO_2 = 48.9-50.8 wt%; Na_2O+K_2O = 9.6–10.6 wt %) [Le Bas et al. 1986] (Figure 7a). Compared with the bulk rocks of the preceding (A.D. 79 Pompeii) and subsequent (A.D. 472 Pollena) eruptions, SMM samples have lower SiO_2 and Alkalies (Figure 7a), and higher MgO and CaO contents (Figure 7b). Trace element concentration also indicates a poorly variable, nearly homogeneous composition (Figure 7c,d). With respect to the products of A.D. 79
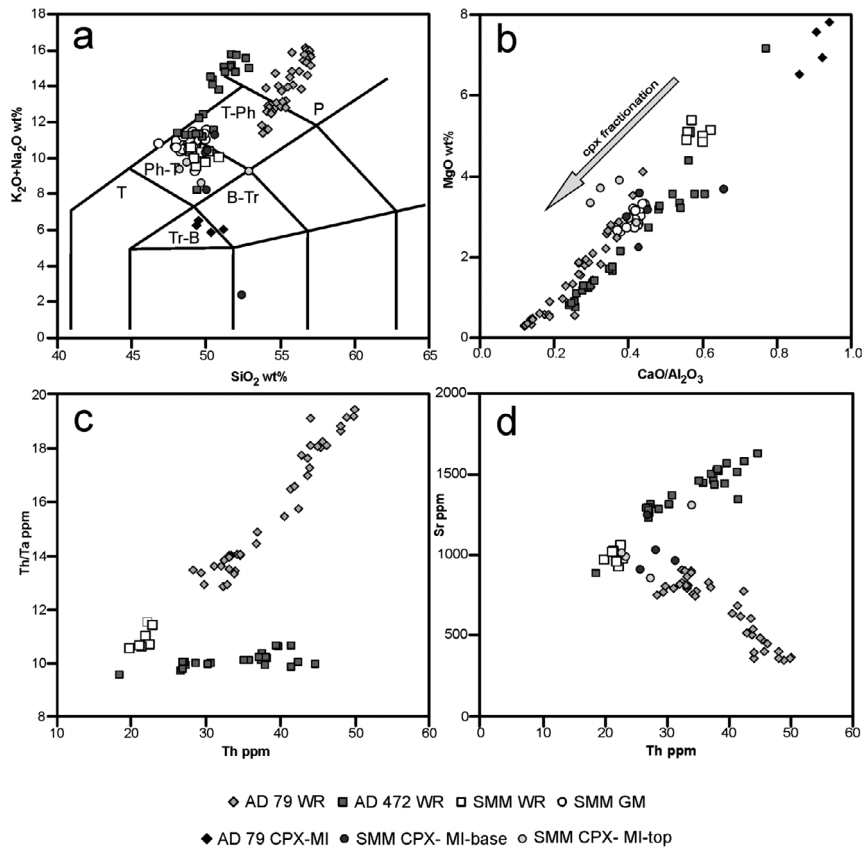
Figure 7. Variation diagrams of major and trace elements in bulk rocks of SMM (white squares), Pompeii (light grey diamonds) and Pollena (grey squares). Matrix glasses and MI of SMM are also reported (white and red circles, respectively) and MI in diospides of Pompei (black diamonds). A) Total alkali *vs* silica diagram [Le Bas et al. 1986]; T, tephrite; Ph-T, phonolitic tephrite; T-Ph, tephritic phonolite; P, phonolite; Tr-B, trachibalsalt; B-Tr, basaltic trachite. C-D) Trace elements variation in bulk rock from SMM compared with Pollena and Pompei rocks. WR, whole rock; GM, groundmass; CPX, clinopyroxene; MI, melt inclusion.

and A.D. 472 eruptions, magma erupted during the SMM shows the lowest contents of incompatible elements (i.e. Ta, Th) and intermediate concentration of compatible elements (i.e. Sr, Ba, Rb). More importantly, the general trends depicted by many trace elements for the products of both the A.D. 79 and A.D. 472 eruptions, clearly converge towards the cluster representing the SMM bulk rocks, so suggesting an important genetic link with the SMM magma (Figure 7c,d).

Melt inclusions

The major element compositions of MI in cpx were corrected for post entrapment host-phase crystallization, using a K_D [(FeO/MgO)cpx/(FeO/MgO)melt] for the potassic melt of 0.27 [Kamenetsky et al. 1995]. As a whole, the extent of post-entrapment crystallization of the host cpx varies between 0 and 10 vol% (Table 2). After correction, the MI in cpx display tephritic phonolite to phonolitic tephrite compositions, with a single MI in the field of basaltic andesite, so covering a relatively wide compositional range (Figure 7a). MI composition shows a general decrease in the CaO/Al_2O_3 ratio from 0.47 to 0.36, passing from the base to the top of the eruption sequence, associated with a slight increase of the MgO

content (Figure 7b). With respect to SMM bulk rock, MI show a compositional trend characterized by lower MgO and CaO, according with the occurrence of pyroxene crystallization. Figures 7c-d show that both major and trace element concentrations in MI overlap those of the less evolved products of the Pompeii eruption (Table 3). By applying the empirical glass-cpx geothermometer of Cioni et al. [1999a] for Vesuvius magmas, we obtain temperatures of 1030-1100 °C at the base of the sequence and of 1028-1060 °C at the top.

Results show that H_2O and CO_2 contents in MI are variable, ranging between 0.84-3.86 wt% and 0-929 ppm, respectively (Figure 8; Table 4). The MI from sample VS 536 (base of Unit H) are distributed in two distinct groups characterized by: a) low H_2O-CO_2, and b) high H_2O-CO_2, roughly plotting along the 220 MPa and 70 MPa isobars, respectively. Conversely, MI from sample VS 537 (top of Unit H) show more scattered values, however still close to the same two isobars. As a whole, the MI from the two samples entirely cover the 1-4 wt.% H_2O range of concentration, while a gap between 300 and 600 ppm of CO_2 is left by the same MI. In the assumption of volatile magma saturation, most of the MI indicate a high CO_2 fugacity of the coexisting fluid

Unit	Unit H base							Unit H top										
sample	536-1-3(2)	536-1-3(3)	536-1-3(1)	536_1_1	536-1-2	VS 536t	VS 536t2	537-1-5	537-1-1	537-1-8	537-1-4	VS 537p	VS 537p2	VS 537s1	VS 537s2	VS 537l	VS 537r1	VS 537r2
SiO_2	50.04	52.63	49.87	50.15	50.61	51.09	50.60	49.81	48.25	52.91	48.61	51.24	49.90	48.80	49.19	50.84	49.19	50.43
TiO_2	0.65	0.73	0.58	1.05	0.81	0.82	0.81	0.64	0.77	0.66	0.87	0.88	0.86	0.96	0.87	0.81	0.99	0.76
Al_2O_3	19.49	20.18	19.40	17.95	19.21	19.33	19.94	19.53	18.85	21.03	19.57	18.96	19.20	18.87	19.12	19.26	18.81	19.24
FeO tot	6.53	7.59	6.18	8.63	6.82	5.64	5.68	6.56	6.93	7.10	6.85	5.43	6.06	6.86	6.97	5.84	7.32	6.02
MnO	0.13	0.20	0.19	0.23	0.20	0.25	0.10	0.16	0.23	0.11	0.16	0.21	0.00	0.22	0.24	0.15	0.11	0.20
MgO	2.09	2.42	2.16	2.45	2.04	2.74	2.52	2.75	2.95	3.22	2.40	2.76	3.00	2.78	2.84	2.44	2.92	2.89
CaO	6.75	6.35	6.10	9.33	7.77	5.94	6.06	6.47	7.22	6.03	7.35	6.19	6.67	7.36	7.09	7.11	6.82	6.00
Na_2O	3.04	0.72	2.98	3.75	3.29	3.81	3.99	2.14	2.50	3.90	2.75	3.75	3.47	3.72	3.68	3.64	3.38	3.46
K_2O	8.38	1.93	8.07	5.47	8.24	9.16	9.14	6.90	7.33	5.44	7.39	9.18	9.41	9.23	9.15	8.85	9.17	9.60
SrO	0.17	0.10	0.04	0.00	0.00	n.d	n.d	0.00	0.00	0.05	0.15	n.d	n.d	n.d	n.d	n.d	n.d	n.d
BaO	0.26	0.27	0.23	0.00	0.00	n.d	n.d	0.20	0.31	0.23	0.30	n.d	n.d	n.d	n.d	n.d	n.d	n.d
F	0.32	0.73	0.33	0.00	0.00	n.d	n.d	0.16	0.44	0.60	0.23	n.d	n.d	n.d	n.d	n.d	n.d	n.d
S	0.20	0.20	0.20	0.00	0.32	0.12	0.05	0.26	0.27	0.26	0.16	0.20	0.19	0.07	0.07	0.09	0.06	0.08
Cl	0.77	0.85	0.91	0.98	0.77	0.82	0.89	0.83	0.78	0.54	0.71	0.89	0.78	0.75	0.72	0.71	0.73	0.89

MI-hosting Pyroxene

	an1	an2	an3	an4	an5	an35	an39	an6	an7	an8	an9	an32	an33	an129	an137	an130	an123	an124
SiO_2	49.86	49.86	49.86	48.69	47.61	48.07	51.17	46.17	46.17	47.11	48.90	50.90	51.38	49.96	49.44	50.87	49.37	51.37
TiO_2	0.75	0.75	0.75	0.94	0.92	0.99	0.74	1.19	1.19	0.82	1.10	0.61	0.63	0.84	0.92	0.58	0.86	0.37
Al_2O_3	5.51	5.51	5.51	5.88	6.04	5.88	3.03	7.52	7.52	5.46	5.43	3.13	2.79	4.39	4.72	4.07	4.92	3.43
MgO	13.94	13.94	13.94	13.52	12.10	12.83	14.88	11.46	11.46	13.75	13.37	14.92	15.64	14.23	14.08	14.86	13.92	15.43
FeO	6.39	6.39	6.39	6.91	8.00	7.21	5.22	9.46	9.46	6.52	7.05	5.19	4.37	5.72	6.36	5.17	6.33	4.66
MnO	0.00	0.00	0.00	0.00	0.00	0.09	0.10	0.47	0.47	0.22	0.00	0.19	0.26	0.16	0.00	0.07	0.18	n.d.
CaO	23.19	23.19	23.19	23.65	24.95	24.51	24.42	23.72	23.72	24.79	23.67	24.62	24.27	24.09	23.86	23.91	23.75	23.99
Na_2O	0.36	0.36	0.36	0.41	0.38	0.28	0.28	0.00	0.00	0.29	0.49	0.35	0.33	0.46	0.47	0.34	0.49	0.44
Wo	48.74	48.74	48.74	49.42	51.94	51.07	49.63	50.41	50.41	50.58	49.54	49.80	49.08	49.82	49.28	49.17	49.42	48.86
En	40.77	40.77	40.77	39.31	35.06	37.20	42.09	33.89	33.89	39.04	38.94	42.00	44.02	40.95	40.47	42.53	40.30	43.73
Fs	10.48	10.48	10.48	11.27	13.00	11.73	8.28	15.69	15.69	10.38	11.52	8.19	6.90	9.23	10.25	8.30	10.28	7.41
PEC (%)	9	10	7	11	2	12	0	5	5	1	4	13	8	8	10	12	7	14
K_D	0.27	0.27	0.27	0.27	0.27	0.27	0.27	0.27	0.27	0.28	0.27	0.27	0.27	0.27	0.27	0.27	0.27	0.27

Restored composition

	an1	an2	an3	an4	an5	an35	an39	an6	an7	an8	an9	an32	an33	an129	an137	an130	an123	an124
SiO_2	50.02	52.35	49.87	49.99	50.55	51.17	50.60	49.65	48.16	52.85	48.62	51.33	49.98	48.98	49.27	50.89	49.23	50.56
TiO_2	0.66	0.73	0.59	1.04	0.82	0.74	0.81	0.66	0.79	0.66	0.88	0.88	0.84	0.94	0.86	0.80	0.98	0.71
Al_2O_3	18.23	18.71	18.43	16.62	18.95	17.61	19.94	18.99	18.34	20.87	19.00	17.14	18.01	17.73	17.79	17.57	17.91	17.31
FeO tot	5.33	6.10	5.04	6.90	5.50	5.47	5.68	5.44	5.72	5.69	5.54	5.22	6.00	6.81	6.86	5.76	7.26	5.85
MnO	0.12	0.18	0.18	0.20	0.20	0.14	0.10	0.15	0.22	0.11	0.15	0.19	0.01	0.22	0.24	0.14	0.11	0.17
MgO	3.16	3.57	2.98	3.67	2.24	7.93	6.06	3.69	3.88	3.33	2.84	8.26	8.00	8.61	8.63	8.90	7.93	8.21
CaO	8.23	8.03	7.30	10.91	8.12	4.15	2.52	6.20	6.92	6.22	8.00	4.30	3.88	3.62	3.88	3.80	3.64	4.43
Na_2O	2.80	0.68	2.80	3.38	3.23	3.40	3.99	2.04	2.39	3.86	2.66	3.29	3.24	3.47	3.39	3.34	3.19	3.09
K_2O	7.63	1.74	7.51	4.87	8.08	8.31	9.14	6.59	7.00	5.39	7.09	8.14	8.71	8.56	8.32	7.89	8.58	8.42
F	0.29	0.66	0.31	0.00	0.00	n.d.	n.d.	0.15	0.42	0.59	0.22	n.d.	n.d.	n.d.	n.d.	n.d.	n.d.	n.d.
S	0.18	0.18	0.19	0.00	0.31	0.12	0.05	0.25	0.26	0.26	0.15	0.19	0.18	0.06	0.06	0.09	0.06	0.07
Cl	0.70	0.77	0.85	0.87	0.75	0.75	0.89	0.79	0.74	0.53	0.68	0.76	0.72	0.69	0.66	0.60	0.69	0.78

Table 2. EPMA compositions of melt inclusions and MI-hosting pyroxenes. PEC (%) is post-entrapment pyroxene crystallization calculated with a K_D value of 0.27 at NNO+1.

Unit	Unit B	Unit H base			Unit H top			
ppm	534-1	536-1-1	536-1-3a	536-1-3b	537-1-1a	537-1-1b	537-1-3c	537-1-4
Li	47.15	42.77	24.6	22.55	17.48	30.82	63.03	22.13
B	39.03	25.87	26.98	29.68	30.94	35.73	44.95	30.46
Sc	12.25	10.54	10.59	5.53	10.06	_	6.07	5.88
V	205.37	228.59	161.81	145.46	162.64	131.37	193.89	193.52
Cr	_	49.21	67.72	_	_	_	_	_
Co	17.66	20.38	18.82	17.86	16.99	20.02	16.81	19.04
Ni	19.89	25.79	9.44	11.35	33.48	17.58		16.34
Zn	69.41	121.63	71.09	85.72	72.21	84.17	102.94	77.87
Rb	290.93	412.14	336.66	288.22	278.67	260.65	532.19	237.86
Sr	1006.49	1383.88	1069.86	1030.19	948.87	1453.29	1124.11	1097.53
Y	23.63	36.05	16.05	19.75	22.41	23.31	26.93	19.86
Zr	231.31	311.04	176.33	241.44	257.86	260.74	255.11	203.54
Nb	42.33	51.8	52.77	48.1	41.03	60.07	40.36	46.24
Cs	17.95	18.2	15.59	15.05	17.51	12.72	36.26	9.18
Ba	1509.52	2477.6	2021.88	1723.22	1527.56	2683.08	2065.22	1845.47
La	69.08	95.79	59.16	71.92	78.83	72.13	74.37	61.3
Ce	134.7	183.94	109.48	126.66	135.69	130.26	136.15	125.12
Pr	16.25	18.65	10.3	13.26	14.99	12.86	16.65	12.02
Nd	54.67	69.5	35.18	46.55	49.89	51.69	60.39	46.72
Sm	7.83	14.85	8.95	6.17	8.2	9.93	7.58	4.8
Eu	1.79	1.92	1.15	1.57	2.12	3.12	3.24	1.77
Gd	6.58	11.62	2.97	5.78	7.74	8.92	7.93	3.63
Tb	0.95	1.22	0.92	0.67	0.83	0.77	0.38	0.569
Dy	7.43	4.96	4.02	4.21	4.67	5.78	6.86	3.81
Ho	0.93	0.46	0.43	0.59	0.85	1.18	1.68	0.78
Er	3.52	5.32	2.87	1.52	2.25	2.2	4.85	1.95
Tm	0.191	0.34	0.082	0.36	0.211	0.333	0.28	0.089
Yb	2.86	1.94	1.8	2.36	2.96	3.32	4.31	1.25
Lu	0.37	0.47	0.16	0.243	0.247	0.214	0.148	0.417
Hf	7.13	5.44	3.41	5.72	6.02	5.18	8.18	3.99
Ta	1.33	1.83	2.66	2.04	2.46	2.75	2.22	2.03
Pb	55.71	48.07	51.41	49.26	50.17	60.6	52.6	63.66
Th	28.51	29.83	34.73	28.15	30.45	37.76	25.19	26.01
U	9.67	10.42	14.09	9.99	10.71	13.47	9.52	10.38

Table 3. Selected compositions of trace elements in melt inclusions by LA-ICP-MS.

(CO_2/ H_2O ratio higher than 0.6). The high CO_2 fugacity of the magmatic fluids and the large spread in the H_2O content at a similar CO_2 concentration in the MI are in agreement with a process in which CO_2-rich vapor percolates through the system from below, being released by magma degassing deeper in the system [Rust et al. 2004, Spilliaert et al. 2006] or by fluids derived from magma-carbonate interaction [Dallai et al. 2011].

Groundmass glasses

Groundmass glasses are rather homogeneous in composition (on average SiO_2: 48.69 wt%, total alkali: 10.73 wt%) (Figure 7a,b). With respect to bulk rock composition, glass is depleted in MgO, K_2O, CaO contents, slightly enriched in Al_2O_3 and Na_2O and with a similar SiO_2 content (Table 2). Mass balance calculations, assuming a simple crystal fractionation process, suggest a

Label	H$_2$O (wt%)	CO$_2$ (ppm)	P (MPa)
vs536t	1.50	249	69
vs536v	0.84	273	72
536-1-3	3.78	757	216
536_1_1	3.35	824	219
536-1-2	3.37	887	224
537-1-5	3.86	869	232
537-1-1	2.73	644	170
537-1-8	2.39	838	183
537-1-4	2.33	278	95
vs537p1	1.96	159	61
vs537r1	0.98	783	169
vs537r1d	1.42	615	146
vs537s1	1.61	929	193
vs537u1	1.84	283	76
vs537l1	1.38	0	32

Table 4. H$_2$O and CO$_2$ concentrations in melt inclusions by FTIR analyses after correction for post entrapment crystallization. P (MPa) was derived from the model of Papale et al. [2006].

37 wt. % crystallization (19% cpx and 18% of lct) to pass from the initial melt composition (bulk composition is here assumed as representative of melt composition) to the less evolved groundmass glass composition, and a further 10% crystallization (6% of cpx, 3 % of pl, 1% of lct) to reach the composition of the most evolved groundmass glass. These calculations are in general agreement with the observed groundmass crystal content. The composition of volatiles dissolved in the groundmass glasses was estimated by EPMA analyses (water content estimated by the difference method,
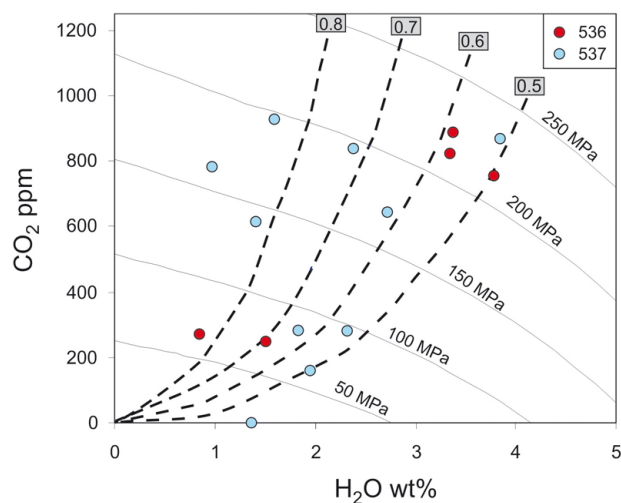
Figure 8. Variation of CO$_2$ and H$_2$O dissolved in melt inclusions. Isobars and the curves showing the pressure-related CO$_2$ *vs* H$_2$O evolution are calculated for the average basaltic composition of melt inclusions using Papale's updated model [Papale et al. 2006].

Devine et al. [1995]) (Table 5). Results indicate a high, although largely scattered H$_2$O content (1.58±0.74 wt.%), and high Cl (1.04±0.11 wt.%). With respect to the most primitive inclusions, this residual water content corresponds to a water loss of at least 75 wt. %. The high Cl content is in agreement with a crystallization of 40 vol% of microlites, suggesting that Cl did not degassed during ascent, a behavior similar to that observed in the groundmass glass of many other Vesuvius eruptions [Santacroce et al. 2008, Cioni et al. 2011].

Discussion

Renewal of volcanic activity after a large eruption

The sporadic information derived from the historical accounts on the activity of the A.D. 79-472 period has been integrated with the results of a detailed stratigraphic-volcanologic study. By comparing available data from historical reports and the stratigraphy of the products, it appears clear that the activity described in the historical documents only represents a small portion of the total activity that characterized the A.D. 79-472 period. Historical accounts are in this case biased toward the description of larger scale activity (violent strombolian events), so masking the occurrence of the long-lasting phases of low-intensity, ash dominated activity.

Field studies evidenced that SMM products were deposited (on the slopes of the volcano) over the final, ash dominated deposits of the A.D. 79 eruption, locally channeled or slightly reworked. This is in a good agreement with the suggestion of several authors [Kuhry 1988, Evans 1993] that the processes of reforestation, in the case of large eruptions devastating the original vegetation, can require more than 100 years, depending on factors such as the local climate, the stability of the flanks and the superficial morphology of the ground. Pollinic studies on samples related to the A.D. 79–SMM interface confirm that, although a minimum amount of pollen material was detected, this represents only the attempt to restore "normal" vegetation conditions [Andronico and Grassi 1998].

On the whole, this information is in accordance with an early resumption of the eruptive activity after the Pompeii eruption. On the contrary, the thickness of the soil formed after the last volcanic event of the SMM cycle suggests the occurrence of a prolonged period of dormancy, possibly lasting more than a century, before activity resumed.

According to the historical accounts, we suggest that activity was concentrated in the first 2 centuries after the A.D. 79 eruption: the strong activity described by Dio Cassius in A.D. 203 can be tentatively related to the lapilli bed of Unit B, close to the base of the prod-

(wt%)	g1	g2	g3	g4	g5	g6	g7	g9	g10	g21	g26
SiO$_2$	48.84	49.25	48.25	49.17	50.00	49.24	48.72	48.77	49.88	49.19	48.40
TiO$_2$	0.91	0.73	0.76	0.81	0.90	0.83	0.86	0.83	0.84	0.83	0.77
Al$_2$O$_3$	17.72	18.02	18.28	17.88	18.22	17.75	17.35	17.79	17.94	17.36	17.91
FeO tot	8.21	8.10	7.98	8.25	7.74	8.32	8.28	8.31	7.62	7.76	8.08
MnO	0.22	0.21	0.19	0.27	0.20	0.16	0.26	0.17	0.20	0.24	0.18
MgO	2.88	2.83	2.75	2.81	2.63	2.79	3.14	3.09	2.99	3.23	2.72
CaO	7.56	7.33	7.54	7.65	6.91	7.50	7.53	7.60	7.48	7.72	6.49
Na$_2$O	5.13	5.04	4.68	5.02	5.08	5.16	4.88	5.11	5.03	4.67	5.58
K$_2$O	5.77	5.67	5.71	5.72	6.49	5.83	5.47	5.28	5.96	4.63	5.63
P$_2$O$_5$	0.61	0.63	0.57	0.61	0.59	0.62	0.73	0.63	0.56	0.67	0.83
Cl	1.10	1.08	0.99	1.12	0.73	1.10	1.10	1.06	1.06	0.92	1.15
CaO/Al$_2$O$_3$	0.43	0.41	0.41	0.43	0.38	0.42	0.43	0.43	0.42	0.45	0.36
Na$_2$O+K$_2$O	10.90	10.71	10.39	10.74	11.58	10.99	10.35	10.39	11.00	9.30	11.21

Table 5. Major element concentration in residual glasses of selected ash fragments belonged to the Unit B (S1).

ucts of the eruptive activity, that was still on-going in the period A.D. 222-235. Radiometric dating on paleosol and charcoals underlying the A.D. 472 deposits give a ^{14}C age of 1630±50 years, that corresponds to a calendar age in the time span between A.D. 350-500 [Santacroce et al. 2008]. The older age could represent the beginning of process responsible for the soil development.

Eruption dynamics

The thick sequence of ash and lapilli-bearing units of the SMM records a long-lived activity characterized by short pulses of relatively high intensity (violent strombolian events) alternated with periods dominated by ash emission. The poor direct historical information on the eruptive activity is possibly biased only toward the most intense phases. The more complete stratigraphic sections suggest that the activity was characterized by several events (according to the nomenclature proposed by Jenkins et al. [2007]) separated by at least four quiescent periods, recorded within the deposits by erosive surfaces. During each event a complex alternation of activity occurred (*multi-stage activity*), with events of highest intensity (violent strombolian activity) alternated with prolonged ash emission activity. The high frequency of the activity inhibited the development of soils or simply the onset of pedogenesis of the ash layers.

Magma fragmentation mechanisms and the role played by the involvement of external water in the eruption dynamics can be discussed basing on the morphological and textural features of lapilli and ash products. The predominance of fluidal and highly vesicular fragments over the blocky, dense clasts in the lapilli layers is an evidence of pure magmatic fragmentation. However, the presence of accretionary lapilli, glass alteration, ad-

hering ash on the external surface of the clasts, and the abundance of blocky morphologies in the ash-bearing bed at the base of the eruption sequence (Unit A), suggest that processes of magma-water interaction were important especially at the beginning of the eruption cycle.

The scarcity of lithic fragments, together with the absence of clasts clearly derived from the two main regional aquifers (respectively hosted in the Mesozoic carbonates and the lavic basement) [Santacroce 1987, Barberi et al. 1989] in the ash beds possibly related to hydromagmatic activity (Unit A) suggest that magma-water interaction possibly involved a very shallow or superficial water body.

The prosecution of the eruption led to a stabilization of the conditions within the volcanic system (and possibly to the exhaustion of the available external fluids) and the evidence of water interaction disappears moving to the top of the sequence. The lapilli beds correspond to violent strombolian events characterized by the generation of quasi-steady, up to few kilometres-high, sustained convective columns [Cioni et al. 2008].

The deposits of several eruptive events with a similar type of activity are also present in the pyroclastic successions interbedded between the deposit of A.D. 472 and A.D. 1631 [Cioni et al. 2008, D'Oriano et al. 2011]. We suggest that the frequent alternation, observed at Vesuvius, between ash-dominated phases of activity and short violent strombolian events can be triggered by variations in the shallow conditions of the magma column rising in the conduit. As observed for similar eruptions of Vesuvius [D'Oriano et al. 2011], we suggest that the continuous generation of ash-laden convective plumes forming the ash layers can be related to the developing of a permeable network within the magma,

while the arrival of a large volume of volatile-rich magma batch (closed-system ascent) was the possible trigger for the shifting of the eruption style from ash-dominated to violent strombolian [Cioni et al. 2011].

Evidence of upward migration of the magma chamber

Compositional and textural data collected on the explosive products erupted during the different phases of the SMM cycle help interpreting the main processes involved in pre-eruptive magma evolution, syn-eruptive magma ascent, and dynamics of eruption activity.

Important suggestions on the evolution of the Vesuvius magmatic system in this period of activity derive from the comparison of the compositional data on the SMM products and those of the two largest eruptions, A.D. 79 and A.D. 472, that respectively preceded and followed the activity. Scaillet et al. [2008] demonstrated that during this period a fundamental change occurred in the geometry of the volcano-magmatic system, with a shift of the position of the main magma reservoir from a general depth of 7-8 km (active from about 20 to 2 ka) to depths of about 3-4 km, roughly corresponding to pressure values of about 220 and 100 MPa, respectively. Data from the metasomatized carapace of the A.D. 472 Pollena eruption give a similar indication [Fulignati and Marianelli 2007]. The compositional data on the SMM products can help in a better understanding of the timing and causes of this important change.

Bulk rock analyses show that during the entire eruption cycle magma composition did not change. The scarcity of phenocrysts also suggests that magma was nearly aphyric (and possibly at a near-liquidus state) while groundmass was (variably) crystal-rich throughout the entire eruption, in agreement with the variable, more evolved, composition of the residual glass.

The general trends depicted by the products of the two large eruptions bracketing the SMM period (both for major and for trace elements) show an unequivocal convergence toward the field occupied by the SMM products, suggesting a common line of descent from them. While the A.D. 79 compositional variations have been interpreted as mainly derived by processes of syn-eruptive magma mixing [Sigurdsson et al. 1990, Cioni et al. 1995], the Pollena magma was dominated by crystal fractionation of cpx, san and lct [Fulignati and Maria-nelli 2007, Santacroce et al. 2008] Despite the contrasting processes which dominated evolution inside the magma reservoirs of the A.D. 79 and 472 eruptions, the SMM magma compositional features clearly suggest that the mafic end-member of these two eruptions was common and that the nature of the deep feeding magma possibly remained un-

changed in this period. On the other hand, the generally large groundmass crystal content of the juvenile material well agrees with the complex, long-lasting style of activity of the SMM period, during which extensive processes of syn-eruptive magma degassing and crystallization possibly occurred.

Important suggestions about the timing of the upward shift of the shallow reservoir between the A.D. 79 and A.D. 472 eruptions proposed by Scaillet et al. [2008] can be derived from volatile data on MI. The cpx phenocrysts hosting the MI show a recurrent diopside-salite zoning which possibly reflects important thermal fluctuations due to the repeated inputs of hot, mafic magma in a small reservoir hosting a slightly more evolved, resident magma [Santacroce et al. 1994, Cioni et al. 1998]. The indication of two main pressures of MI entrapment derived from volatiles data can be interpreted as an evidence of possible recycling of a mafic residual of the A.D. 79 eruption, crystallized in a reservoir at 7-8 km depth [Balcone-Boissard et al. 2008, Scaillet et al. 2008] successively injected by newly arrived deep magma and transported in a shallower reservoir (around 4 km), from which the magma was erupted. According to this interpretation, the upward shift of the reservoir evidenced by the experimental petrology data of Scaillet et al. [2008] occurred immediately after the A.D. 79 eruption, possibly related to the caldera collapse occurred during this eruption, which profoundly modified the summit portion and the roots of the volcanic edifice (differently for example from the preceding 3900 ka Avellino eruption, during which a large caldera structure formed in correspondence of the Piano delle Ginestre, on the west flank of the Somma volcano) [Cioni et al. 1998].

Conclusions

The study of the pyroclastic succession occurring between the A.D. 79 Pompeii and A.D. 472 Pollena eruptions, named the SMM eruption cycle, allowed to define accurately the style of activity and the main features of the magmatic system which characterized the onset of the last 2000 years of Vesuvius history.

The studied deposits are related to a prolonged period of activity, possibly spanning at least 20-30 years during the third century, during which low-intensity, continuous ash emission activity alternated with short-lived stages of more intense, violent strombolian activity. The juvenile material differs markedly from the more evolved products of A.D. 79 or the A.D. 472 products, and the composition is constant and mafic throughout the whole eruption, suggesting that magma chamber dynamics was dominated by mafic magma recharge from the deep rather than temperature decrease and magma

evolution (young stage of Cioni et al. [1998]).

Data from historical accounts and ^{14}C ages suggest that the volcano, after the A.D. 79 paroxysm, remained inactive for about a century; a new, shallower magma reservoir formed, possibly related to the important structural changes induced in the volcanic system by the caldera collapse, and after the onset of SMM activity open conduit conditions rapidly established. Activity was followed by a prolonged (more than one century) quiescence that preceded the A.D. 472 Pollena subplinian eruption.

Volatiles data help constraining the timing of establishment of the shallower level reservoir that characterized all the post A.D. 79 activity. The shallower depth of this new magma reservoir was possibly one of the main factors which caused the passage from the low frequency, high magnitude activity which characterized the period between 20 and 2 ka, to the high frequency, low magnitude activity of the last 2000 years of Vesuvius.

References

Alfano, G.B. (1923). Le eruzioni del Vesuvio tra il 79 e il 1631, Comunicazione letta nella seduta sezionale dell'associazione del 13 settembre 1923, 32 pp.

Alfano, G.B., and I. Friedlander (1929). La storia del Vesuvio illustrata dai documenti coevi, Naples, K. Holm, 71 pp.

Andronico, D., and R. Grassi (1998). Vegetation colonization after a volcanic event: an example from Vesuvio (Naples), In: International Symposium on "Paleodiversifications: Land and Sea Compared" (Lyon, France, July 6-8, 1998), Abstracts.

Andronico, D., and R. Cioni (2002). Contrasting styles of Mount Vesuvius activity in the period between the Avellino and Pompeii plinian eruptions, and some implications for assessment of future hazards, Bull. Volcanol., 64, 372-391.

Arnò, V., C. Principe, M. Rosi, R. Santacroce, A. Sbrana and M.F. Sheridan (1987). Eruptive history, In: R. Santacroce (ed.), Somma-Vesuvius, Quaderni de "La Ricerca Scientifica", CNR, 114, 53-103.

Arrighi, S., C. Principe and M. Rosi (2001). Violent strombolian and subplinian eruptions at Vesuvius during post-1631 activity, Bull. Volcanol., 63, 126-150.

Balcone-Boissard, H., B. Villemant, G. Boudon and A. Michel (2008). Non-volatile vs volatile behaviours of halogens during the A.D. 79 plinian eruption of Mt. Vesuvius, Italy, Earth and Planet Sci. Lett., 269, 66-79.

Barberi, F., R. Cioni, M. Rosi, R. Santacroce, A. Sbrana and R. Vecci (1989). Magmatic and phreatomagmatic phases in explosive eruptions of Vesuvius as deduced by grain-size and compositional analysis of pyroclastic deposits, J. Volcanol. Geoth. Res., 38, 287-307.

Cioni, R., A. Sbrana and R. Vecci (1992). Morphologic features of juvenile pyroclasts from magmatic and phreatomagmatic deposits of Vesuvius, J. Volcanol. Geoth. Res., 51, 61-78.

Cioni, R., L. Civetta, P. Marianelli, N. Metrich, R. Santacroce and A. Sbrana (1995). Compositional layering and syneruptive mixing of a periodically refilled magma chamber: the A.D. 79 plinian eruption of Vesuvius, J. Petrol., 36, 739-776.

Cioni, R., P. Marianelli and R. Santacroce (1998) Thermal and compositional evolution of the shallow magma chambers of Vesuvius: Evidence from pyroxene phenocrysts and melt inclusions, J. Geophys. Res., 103, 277-294.

Cioni, R., P. Marianelli and R. Santacroce (1999a). Temperature of Vesuvius magmas, Geology, 27, 443-446.

Cioni, R., R. Santacroce and A. Sbrana (1999b). Pyroclastic deposits as a guide for reconstructing the multi-stage evolution of the Somma-Vesuvius Caldera, Bull. Volcanol., 6, 207-222.

Cioni, R. (2000). Volatile content and degassing processes in the A.D. 79 magma chamber at Vesuvius (Italy), Contr. Mineral. Petrol., 140, 40-54.

Cioni, R., A. Bertagnini, R. Santacroce and D. Andronico (2008) Explosive activity and eruption scenarios at Somma-Vesuvius (Italy): a review, J. Volcanol. Geoth. Res., 178, 331-346.

Cioni, R., A. Bertagnini, A. Andronico, P.D. Cole and F. Mundula (2011). The 512 A.D. eruption of Vesuvius: complex dynamics of a small scale subplinian event, Bull. Volcanol., 73, 789-810.

Dallai, L., R. Cioni R., C. Boschi and C. D'Oriano (2011). Carbonate-derived CO_2 purging magma at depth: influence on the eruptive activity of Somma-Vesuvius, Italy, Earth Planet. Sci. Lett., 310, 84-95.

Dellino, P., and L. La Volpe (1996). Image processing analysis in reconstructing fragmentation and transportation mechanism of pyroclastic deposits. The case of Monte Pilato–Rocche Rosse eruptions, Lipari (Aeolian islands, Italy), J. Volcanol. Geoth. Res., 71, 13-29.

Devine, J.D., J.E. Gardner, H.P. Brack, G. Lyne and M.J. Rutherford (1995). Comparison of microanalytical methods for estimating H_2O contents of silicic volcanic glasses, Am. Mineral., 80, 319-328.

Dio Cassius. Historiae Romanae quae supersunt, The Loeb Classical Library, Harvard Univ. Press, Cam-

bridge, MA, 1925. Hamburg, II, p. 1272.

D'Oriano, C., S. Da Pelo, F. Podda and R. Cioni (2008) Laser-Ablation Inductively Coupled Plasma Mass Spectrometry (LA-ICP-MS): setting operating conditions and instrumental performance, Per. Mineral., 77, 65-74.

D'Oriano, C., R. Cioni, A. Bertagnini, D. Andronico and P.D. Cole (2011). Dynamics of ash-dominated eruptions at Vesuvius: the post-512 ad AS1a event, Bull. Volcanol., 73, 699-715.

Evans, S.P. (1993). Can northern hemisphere Holocene volcanic events be recorded in pollen data?, Il Quaternario, 8 (1), 119-138.

Fierstein, J., and M. Nathenson (1992). Another look at the calculation of fallout tephra volumes, Bull. Volcanol., 54, 156-167.

Fulignati, P., and P. Marianelli (2007). Tracing volatile exsolution within the 472 "Pollena" magma chamber of Vesuvius (Italy) from melt inclusions, J. Volcanol. Geoth. Res., 161, 289-302.

Galenus, C. De methodo medendi Libri XIII, Venetiis, apud Juntas, 1609, vol. V, chapter 12.

Hammer, J.E., and M.J. Rutherford (2002). An experimental study of the kinetics of decompression-induced crystallization in silicic melt, J. Geophys. Res., 107 (B1); doi:10.1029/2001JB000281.

Heiken, G., and K.H. Wohletz (1985) Volcanic Ash, University of California Press, Berkeley, California, 245 pp.

Heiken, G., and K.H. Wohletz (1991). Fragmentation processes in explosive volcanic eruptions, In: R.V. Fisher and G. Smith (eds.), Sedimentation in Volcanic Settings, Soc. Econ. Paleont. and Mineral. Spec. Pub., 45, 19-26.

Houghton, B.F., and C.J.N. Wilson (1989) A vesicularity index for pyroclastic deposits, Bull. Volcanol., 51, 451-462.

Jenkins, S.F., C.R. Magill and K.J. McAneney (2007). Multi-stage volcanic event: a statistical investigation, J. Volcanol. Geoth. Res., 161, 275-288.

Joron, J.L., M. Truil and L. Raimbault (1997). Activation analysis as a geochemical tool: Statement of its capabilities for geochemical trace element studies, H. Radioan. Nucl. Ch., 216, 229-235.

Kamenetsky, V., N. Metrich and R. Cioni (1995). Potassic primary melts of Vulsini (Roman Province): evidence from mineralogy and melt inclusions, Contrib. Mineral. Petrol., 120, 186-196.

Kuhry, P. (1988). A paleobotanical and palynological study of Holocene peat from the El Bosque mire, located in a volcanic area of the Central Cordillera of Colombia, Rew. Palaeobot. Palynol., 55, 19-72.

Le Bas, M.J., R.W. Le Maitre, A. Streckeisen and B. Zan-

nettin (1986). A chemical classification of volcanic rocks based on the total alkali-silica diagram, J. Petrol., 27, 745-750.

Lirer L., T. Pescatore, B. Booth and G.P.L. Walker (1973). Two Plinian Pumice-Fall Deposits from Somma-Vesuvius, Italy, Bull. Geol. Soc. Amer., 84, 759-772.

Maiolo, S. (1615). Dies caniculares: hoc est colloquia phisica, Moguntiae lib. I colloquio 168, De montibus, 287.

Marianelli, P., N. Metrich and A. Sbrana (1999). Shallow and deep reservoir involved in magma supply of the 1944 eruption of Vesuvius, Bull. Volcanol., 61, 48-63.

Mecatti, G. (1754). Discorsi storici-filosofici sopra il Vesuvio, Napoli, di Simone, XLVII.

Mele, D., R. Sulpizio, P. Dellino and L. La Volpe (2011). Stratigraphy and eruptive dynamics of a pulsating Plinian eruption of Somma-Vesuvius: the Pomici di Mercato (8900 years B.P.), Bull. Volcanol., 73, 257-278.

Palmieri, L. (1887). Il Vesuvio e la sua storia, In: Lo spettatore del Vesuvio e dei Campi Flegrei, Napoli, 7-33.

Papale, P, R. Moretti and D. Barbato (2006). The compositional dependence of the saturation surface of $H_2O + CO_2$ fluids in silicate melts, Chemical Geology, 229, 78-95.

Principe, C., J.C. Tanguy, S. Arrighi, A. Paiotti, M. Le Goff and·U. Zoppi (2004). Chronology of Vesuvius activity from A.D. 79 to 1631 based on archeomagnetism of lavas and historical sources, Bull. Volcanol., 66, 703-724.

Pyle, D.M. (1989). The thickness, volume and grainsize of tephra fall deposits, Bull. Volcanol., 51, 1-15.

Rolandi, G., G. Mastrolorenzo, A.M. Barrella and A. Borrelli (1993). The Avellino plinian eruption of Somma-Vesuvius (3760 y. B.P.); the progressive evolution from magmatic to hydromagmatic style, J. Volcanol. Geoth. Res., 58, 67-88.

Rolandi, G., P. Petrosino and J. Mc Geehin (1998). The interplinian activity at Somma-Vesuvius in the last 3500 years, J. Volcanol. Geoth. Res., 82, 19-52.

Rosi, M., and R. Santacroce (1983). The A.D. 472 'Pollena' eruption, volcanological and petrological data for this poorly known plinian-type event at Vesuvius, J. Volcanol. Geoth. Res., 17, 249-271.

Rust, A.C, K.V. Cashman and P.J. Wallace (2004) Magma degassing buffered by vapor flow through brecciated conduit margins, Geology, 32, 349-352.

Santacroce, R. (1987). Somma-Vesuvius, Quaderni de "La Ricerca Scientifica", CNR, 114 (Progetto finalizzato Geodinamica, Monografie finali, 8), 251 pp.

Santacroce, R., R. Cioni, L. Civetta, P. Marianelli, N. Metrich and A. Sbrana (1994). How Vesuvius works, Atti della Accademia Nazionale dei Lincei, 112, 185-196.

Santacroce, R., A. Sbrana, D. Andronico, R. Cioni, A.

Di Vito, P. Marianelli, R. Sulpizio, G. Zanchetta, S. Arrighi, E. Benvenuti, L. Gurioli, F.M. Leoni and W. Luperini (2003). Carta Geologica del Vesuvio, scala 1:15.000, S.EL.CA., Firenze.

Santacroce, R, R. Cioni, P. Marianelli, A. Sbrana, R. Sulpizio, G. Zanchetta, D.J. Donahue and J.L. Joron (2008). Age and whole rock-glass compositions of proximal pyroclastics from the major explosive eruptions of Somma-Vesuvius: A review as a tool for distal tephrostratigraphy, J. Volcanol. Geoth. Res., 177, 1-18.

Scaillet, B., M. Pichavant and R. Cioni (2008). Upward migration of Vesuvius magma chamber over the past 20, 000 years, Nature, 455, 216-219.

Sigurdsson, H., S. Carey, W. Cornell and T. Pescatore (1985). The eruption of Vesuvius in A.D. 79, Natl. Geogr. Res., 1, 332-387.

Sigurdsson, H., W. Cornell and S. Carey (1990). Influence of magma withdrawal on compositional gradients during the A.D. 79 Vesuvius eruption, Nature, 345, 519-521.

Spilliaert, N., P. Allard, N. Métrich and A.V. Sobolev (2006). Melt inclusion record of the conditions of ascent, degassing, and extrusion of volatile-rich alkali basalt during the powerful 2002 flank eruption of Mount Etna (Italy), J Geophys Res., 111 (B4); doi:10.1029/2005JB003934.

Sulpizio, R., D. Mele, P. Dellinoi and L. La Volpe (2005). A complex, Subplinian type eruption from low-viscosity, phonolitic to tephri-phonolitic magma: the A.D. 472 (Pollena) eruption of Somma-Vesuvius, Italy, Bull. Volcanol., 67, 743-767.

Sulpizio, R., R. Cioni, M.A. Di Vito, D. Mele, R. Bonasia, P. Dellino and L. La Volpe (2010a). The Avellino eruption of Somma-Vesuvius (3.8 ka BP). Part I: stratigraphy, chemistry and eruptive mechanisms, Bull. Volcanol., 72, 539-558.

Sulpizio, R., R. Bonasia, P. Dellino, D. Mele, M.A. Di Vito and L. La Volpe (2010b). The Pomici di Avellino eruption of Somma-Vesuvius (3.9 ka BP). Part II: sedimentology and physical volcanology of pyroclastic density current deposits, Bull. Volcanol., 72, 559-577.

van Achterbergh, E., C.G Ryan, S.E. Jackson and W.L. Griffin (2001). Data reduction software for LA-ICP-MS, In: P. Sylvester (ed.), Laser-ablation-ICPMS in the earth sciences: principles and applications, Mineralogical Association of Canada, Short Course, 29, 239-243.

Wohletz, K.H. (1983). Mechanisms of hydrovolcanic pyroclasts formation: grain-size, scanning electron microscopy, and experimental studies, J. Volcanol. Geoth. Res., 17, 31-64.

*Corresponding author: Raffaello Cioni,
Università di Cagliari, Dipartimento di Scienze della Terra, Cagliari, Italy; email: rcioni@unica.it.